May, 2010

Very High Frequency Channel-Select MEMS Filters Based on Self-Coupled Piezoelectric AlN Contour-Mode Resonators

Chengjie Zuo, *University of Pennsylvania*
Nipun Sinha, *University of Pennsylvania*
Gianluca Piazza, *University of Pennsylvania*

Sensors and Actuators A 160 (2010) 132–140

Contents lists available at ScienceDirect

Sensors and Actuators A: Physical

journal homepage: www.elsevier.com/locate/sna

Very high frequency channel-select MEMS filters based on self-coupled piezoelectric AlN contour-mode resonators

Chengjie Zuo*, Nipun Sinha, Gianluca Piazza

Penn Micro and Nano Systems Laboratory (PMaNS Lab), Department of Electrical and Systems Engineering, University of Pennsylvania, Philadelphia, PA 19104, USA

ARTICLE INFO

Article history:
Received 24 October 2009
Received in revised form 10 March 2010
Accepted 8 April 2010
Available online 28 April 2010

Keywords:
Aluminum nitride (AlN)
Piezoelectric filters
Channel-select filters
Microelectromechanical systems (MEMS)
Contour-mode resonators
Self-coupling

ABSTRACT

This paper reports experimental results on single-chip multi-frequency channel-select filters based on self-coupled piezoelectric aluminum nitride (AlN) contour-mode microelectromechanical (MEMS) resonators. Two-port AlN contour-mode resonators are connected in series and electrically coupled using their intrinsic capacitance to realize multi-frequency (94–271 MHz), narrow bandwidth (~0.2%), low insertion loss (~2.3 dB), high off-band rejection (~60 dB) and high linearity (IIP3 ~100 dBmV) channel-select filters on the same chip. This technology enables multi-frequency, high-performance and small-form-factor filter arrays and makes a single-chip multi-band reconfigurable radio frequency (RF) solution possible in the near future.

1. Introduction

Key issues for the realization of next generation wireless devices are efficient spectral utilization, high level integration and low-power consumption. In order to adaptively make use of the electromagnetic spectrum, a transceiver will need to selectively process radio frequency (RF) signals over a wide frequency range (~10 MHz up to few GHz) and rapidly switch from one band to another. An essential part of this multi-band analog signal processor is an array of multi-frequency narrow-band channel-select filters that can be integrated with other components, like switches and oscillators, to form a single-chip multi-band RF solution.

A recently emerged and very promising technique to design integrated, high-performance and narrow-band filters is based on high quality factor (Q) microelectromechanical (MEMS) resonators. Several research groups have been developing MEMS resonator technologies based on electrostatic [1–3] and piezoelectric [4,5] transduction mechanisms that are capable of providing multiple frequencies of operation on the same silicon substrate, in contrast with conventional Film Bulk Acoustic Resonator (FBAR) or quartz crystal technologies for which only one frequency per substrate is possible. Among these, aluminum nitride (AlN) contour-mode vibrating RF MEMS technology [4] stands out as the most promising one capable of immediately satisfying the critical requirements of the rapidly developing wireless industry. It is currently the only technology that can reliably span a wide frequency range from 10 MHz up to several GHz (operating in the fundamental mode of vibration) on the same silicon chip, and simultaneously offer high Q in air (1000–4000) and low motional resistance (25–700 Ω), which makes the devices readily matched to conventional 50 Ω RF systems. Compared with Silicon-based electrostatic MEMS resonators, a significant advantage of piezoelectric transduction is that low motional resistance and high power handling can be achieved simultaneously, while the motional resistance of electrostatic MEMS resonators is generally much larger due to the relatively lower electromechanical coupling coefficient. Among all the available piezoelectric materials (e.g., PZT and ZnO), AlN is the only material that has been proven post-CMOS compatible and widely used in the wireless communication industry (FBAR filters as duplexers for cell phones [6]). Additionally, among the other piezoelectric materials, thin-film AlN has shown some of the highest k_t^2Q products (figure of merit of a mechanical resonator; k_t^2 is the effective electromechanical coupling coefficient) making it one of the preferred candidates for filter synthesis based on laterally vibrating MEMS resonators.

Employing this piezoelectric AlN contour-mode MEMS technology, very high frequency (VHF) band-pass filters have been demonstrated by electrically coupling one-port resonators in a ladder topology [7]. The implementation of ladder filters requires the ability to fabricate resonators with different resonant frequencies for the series and shunt branches. Depending on the bandwidth

* Corresponding author at: Room 203 Moore Building, 200 South 33rd Street, Philadelphia, PA 19104, USA. Tel.: +1 215 573 3276.
E-mail address: czuo@seas.upenn.edu (C. Zuo).

0924-4247/$ – see front matter © 2010 Elsevier B.V. All rights reserved.
doi:10.1016/j.sna.2010.04.011

specification, a ladder filter may require a relative frequency shift ($\Delta f/f_s$) ranging between 0.1% and 3% in the resonator series resonant frequency, which poses a big challenge on the ultimate achievable yield. Furthermore, in [7] the off-band rejection was measured to be only 27 dB, which can cause severe limitations for channel-select applications. In this work, we propose a new topology to implement multi-frequency (94–271 MHz) channel-select RF MEMS filters with narrow bandwidth (~0.2%), low insertion loss (~2.3 dB), and high off-band rejection (~60 dB) [8]. Three or four two-port AlN contour-mode resonators are connected in series and coupled electrically by their intrinsic capacitance to form high-performance 3rd and 4th order filters, respectively. Compared to the classical ladder filter implementation, this coupling technique reduces the overall device size by employing only half components, improves manufacturing yield by using single-frequency resonators, intrinsically provides narrower bandwidth for channel selection, and, easily increases filter off-band rejection without the need to resort to different size resonators.

2. Resonator and filter design

2.1. Design goals

For the application of channel selection, there are specific design goals that need to be met to synthesize filters based on piezoelectric AlN contour-mode MEMS resonators. First of all, the fractional bandwidth (*FBW*), namely the filter 3 dB bandwidth ($BW_{3\,dB}$) divided by the center frequency (f_c), has to be small enough to really select the desired RF signal channel with very good rejection of adjacent channels. The specifications may vary depending on the particular wireless communication standard. For example, the channel width of the IEEE 802.11a standard is 16.6 MHz at 5 GHz center frequency; correspondingly the fractional channel bandwidth is 0.3% [9]. On the other hand, it is also preferable to pursue narrower channels to develop novel RF architectures for which smaller channel bandwidth may result in higher efficiency of electromagnetic spectral utilization and higher signal-to-noise ratio [1].

Second, low insertion loss is very critical for direct channel selection at RF frequencies. For traditional heterodyne and homodyne (direct-conversion) architectures, channel selection is usually performed at the baseband frequency after the low noise amplifier (LNA) and mixer stages, which relaxes the *Q* requirements on the filters. It is also possible to place the channel-select filter before the mixer, but this is done at the cost of increasing the RF signal gain (therefore power consumption) of the LNA [9]. In all these cases, insertion loss is not a significant issue, since the signal is already amplified before it goes through the channel selector. However, if direct RF channel selection and filtering are carried out before the LNA stage, insertion loss of the channel-select filter becomes the most critical parameter in the receiver chain, since solely 1 dB degradation of the RF signal may result in extra burden on the subsequent stages (LNA, mixer, local oscillator, etc.) in terms of gain, noise figure, and linearity. In order to satisfy the same receiver specification, orders of magnitude more power consumption or chip area occupation may be required to account for the power loss in the first stage. Therefore, the insertion loss of an RF channel-select filter has to be as small as possible.

Finally, the RF channel-select filter should also serve as a bridge to connect the antenna with the transceiver integrated circuits (ICs). Antennas generally have a characteristic impedance around 50 Ω, while transceiver ICs usually work at a higher impedance. Therefore, it is desirable for the channel-select filter to have low device impedance ranging from 50 Ω to several kΩ, so that impedance matching is realized through the filter itself and extra power loss in external matching networks is avoided.

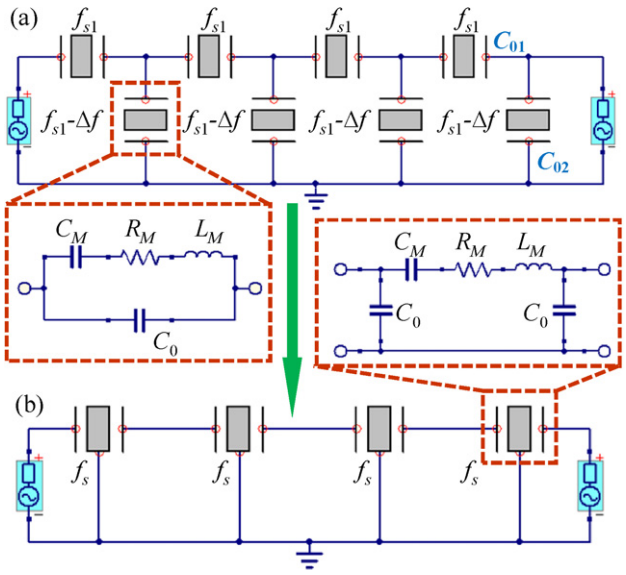

Fig. 1. Equivalent circuit schematics of (a) the ladder topology and (b) the self-coupling technique for the synthesis of a 4th order band-pass filter. The Butterworth Van Dyke (BVD) models for the composing one-port and two-port piezoelectric AlN contour-mode resonators are also given.

These specifications are valid in general and apply also to the VHF filters of this work. Although the demonstrated filters operate in a frequency range below the more conventional cell bands, they can still be employed in lower frequency systems such as TV tuners or as intermediate frequency (IF) stages in heterodyne receivers so as to solve the problem of tuning high-*Q* systems by means of filter banks as proposed by Bakkaloglu and co-workers in [10].

2.2. From ladder to self-coupling topology

The ladder topology has been widely used in electrically coupled filters, e.g., FBAR duplexers [11], electrostatically [12] as well as piezoelectrically [7] transduced band-pass MEMS filters. For an *n*th order filter, 2*n* one-port resonators are needed to form the cascaded L networks, as shown in Fig. 1(a). Among these devices, *n* series resonators have a series resonant frequency at f_{s1} and the other *n* shunt resonators at $f_{s1} - \Delta f$, so that the series resonance of the series branch, f_{s1}, coincides with the parallel resonance of the shunt branch, f_{p2}. The fractional bandwidth of the final filter can be derived to be approximately $8k_t^2/\pi^2$, primarily determined by the effective electromechanical coupling coefficient, k_t^2, while the out-of-band rejection is set by the transducer capacitance ratio (C_{02}/C_{01}, as shown in Fig. 1 and can be calculated using the equation for $C_{0,1}$ in Eq. (1)) of the resonators in the shunt and series branches [7]. In the piezoelectric AlN contour-mode technology, the desired frequency shift Δf was realized by lithographically removing small amounts of Pt electrodes to reduce the mass loading and raise the resonant frequency. This additional process step introduces an additional complication in the micro-fabrication of the filters and can limit the ultimate achievable yield. Furthermore, the out-of-band rejection was found to be ~27 dB causing severe limitations on channel-select applications.

Therefore, based on all these considerations and the design goals described in the previous section, we propose a self-coupling technique that utilizes the intrinsic capacitance existing in two-port AlN contour-mode resonators, so that high-performance narrow-

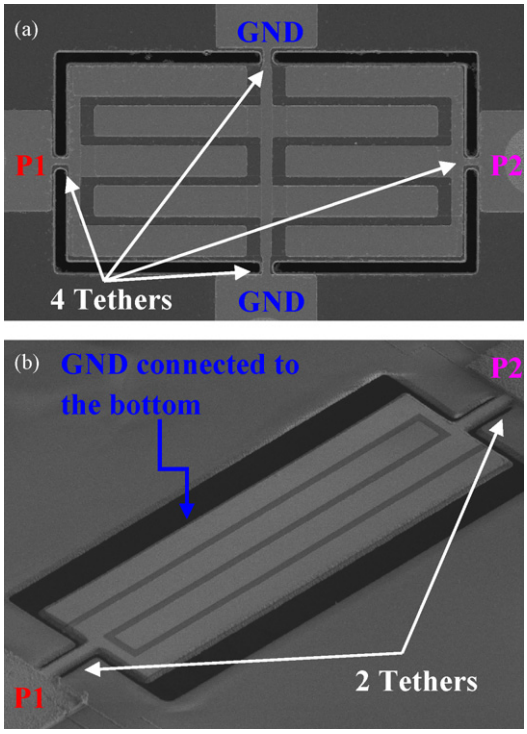

Fig. 2. SEM pictures of the (a) 4-tether design and (b) 2-tether design for a two-port piezoelectric AlN contour-mode resonator. "P1" stands for the input port, while "P2" for the output port of the two-port resonator. "GND" stands for electrical ground.

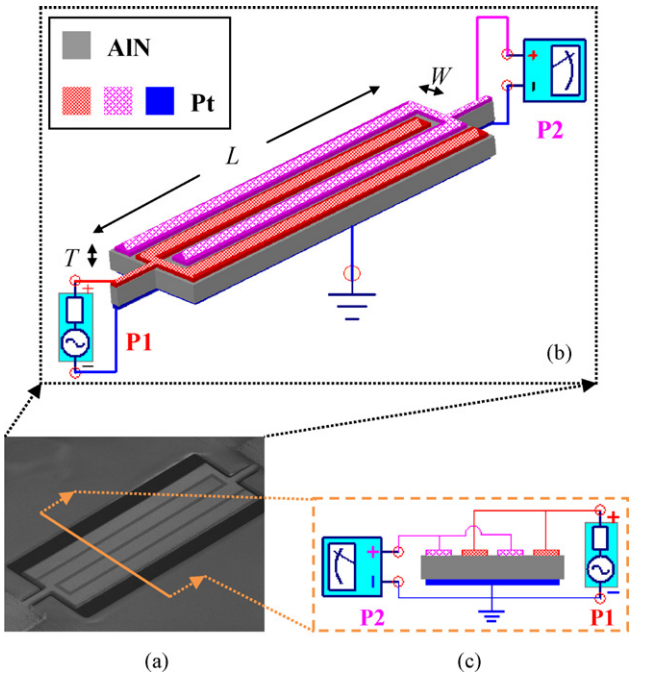

Fig. 3. (a) SEM picture, (b) 3D schematic and (c) cross-sectional schematic of a two-port piezoelectric AlN contour-mode MEMS resonator in the 2-tether interdigitated configuration. A voltage meter is used here at the output port to illustrate the idea of using P2 for sensing and P1 for actuation.

band filters can be formed by cascading several single-frequency resonator stages directly without the need for external coupling elements. Similar topologies based on capacitive coupling of resonator stages have already been demonstrated, but always used external components [13]. At the same time, for an nth order filter, only half the components (i.e., n two-port AlN contour-mode resonators) are needed when compared with the ladder topology. The equivalent circuit schematic for a 4th order self-coupled filter is given in Fig. 1(b). In the following sections, it will also be shown that a much narrower bandwidth of $3k_t^2/\pi^2$ and high out-of-band rejection of 60 dB can be achieved without sacrificing other performances.

2.3. Two-port AlN contour-mode resonators

The design of a two-port AlN contour-mode resonator has been introduced in our previous work [14]. It consists of two sets of one-port sub-resonators: one for input actuation and the other for output sensing, which are modeled to be coupled at infinitely stiff locations and have perfect mechanical energy coupling. As the most intuitive and easiest way of realizing a two-port configuration in higher order contour-mode devices, we first tested a 4-tether design with the input and output ports defined by placing the electrodes on separate halves of the device, as illustrated in Fig. 2(a). However, because there are two tethers fixing the middle part of the piezoelectric plate where the mechanical coupling happens, the acoustic wave propagation between the input and output ports is largely suppressed and therefore the overall device Q deteriorated. This was shown by the measured high insertion loss (IL) of 11.7 dB [14].

Consequently, we have come up with a 2-tether interdigitated configuration to maximize the mechanical energy exchange between the input and output sub-resonators and simultaneously minimize the anchor loss. As shown in Figs. 2(b) and 3, the resonator body consists of a 2 μm piezoelectric AlN film sandwiched between two platinum (Pt) thin-film layers. The bottom Pt layer is a single electrode plate connected to electrical ground (GND), while the top Pt layer is patterned into four parallel electrodes, two of which (red parts in Fig. 3) are connected together to form the input port (P1). The other two connected electrodes (pink parts in Fig. 3) form the output port (P2) of the two-port resonator. (For interpretation of the references to color in this sentence, the reader is referred to the web version of the article.) The device is symmetrical from both electrical and mechanical perspectives, so the roles of the input and output ports can be switched. Since each AlN block with electrodes on two parallel surfaces constitutes a one-port rectangular contour-mode resonator [4], both the input and output ports can be treated as two one-port sub-resonators electrically connected in parallel. Each of the sub-resonators is of length, L, and width, W, as shown in Fig. 3.

In the following analysis, we will assume P1 to be the input actuating port and P2 the output sensing port. When an AC signal is applied to P1 (formed by red and blue electrodes), the vertical electric field across the AlN film induces in-plane dilation or contraction of the resonator body. If the signal frequency coincides with the intrinsic natural frequency of the structure, a contour mode of vibration is excited and the corresponding mechanical strain (therefore stress) is induced in the whole rectangular plate. Because of the direct piezoelectric effect, charge is generated and collected by the sensing electrodes of P2 (formed by pink and blue electrodes). (For interpretation of the references to color in this sentence, the reader is referred to the web version of the article.) The 2D and 3D mode shapes (fundamental width-extensional mode [15]) of the resonator were obtained from COMSOL® FEM simulations and are given in Fig. 4. The non-uniform mode shape along the length of the resonator is caused by the specific aspect ratio of the resonator design in this paper. Further optimization of the resonator geometry will be pursued in future work so as to confine maximum energy within the desired mode of vibration and improve the transducer efficiency.

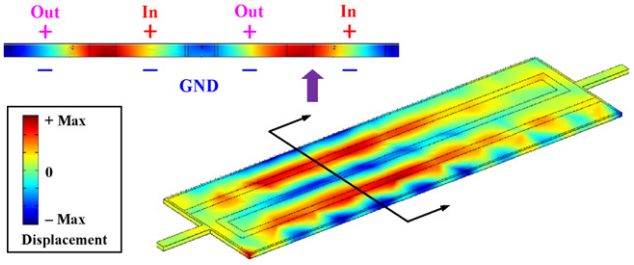

Fig. 4. Resonant mode shapes of the two-port AlN contour-mode resonator (from COMSOL® FEM simulations).

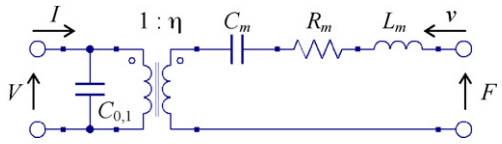

Fig. 5. Equivalent circuit model of a one-port piezoelectric AlN contour-mode resonator.

2.4. Equivalent circuit model

As has been derived in [4], the electrical behavior of a one-port AlN contour-mode resonator can be described by the equivalent circuit shown in Fig. 5. The model uses the analogy between mechanical structures and electrical circuits to replace force (F) by voltage (V) and velocity (v) by current (I). The parameters in the electrical domain are related to those in the mechanical domain by the electromechanical coupling coefficient, η, which is modeled as a transformer in the equivalent circuit to represent the energy conversion between the two domains. For a rectangular sub-resonator with dimensions of $L \times W \times T$ (Fig. 3) operating in its fundamental width-extensional mode, the equivalent parameters can be computed as (assuming a simplified 1D model) [4]:

$$C_{0,1} = \varepsilon_{33}\varepsilon_0 \frac{WL}{T}, \qquad R_m = \frac{\pi}{2} TL \frac{\sqrt{E_{eq}\rho_{eq}}}{Q}, \qquad L_m = \frac{\rho_{eq} LWT}{2},$$

$$C_m = \frac{2}{\pi^2 E_{eq}} \frac{W}{LT}, \qquad \eta = 2d_{31}E_{eq}L, \qquad \omega_s = 2\pi f_s = \frac{\pi}{W}\sqrt{\frac{E_{eq}}{\rho_{eq}}} \quad (1)$$

where ε_0 is the permittivity of free space; ε_{33} is the dielectric constant of AlN in direction 3 (c-axis); L, W and T refer to the length, width and thickness of the sub-resonator, respectively; E_{eq} and ρ_{eq} are the equivalent in-plane elastic modulus and mass density of the AlN–Pt composite; d_{31} is the (3, 1) entry of AlN's d-form piezoelectric coefficient matrix; ω_s is the series resonant frequency.

By applying the equivalent circuit model to both input and output sub-resonators, as illustrated in Fig. 6(a), the combined equivalent circuit for the two-port resonator is given in Fig. 6(b), which assumes perfect mechanical energy exchange between the sub-resonators. All the energy losses in the two-port resonator are lumped together and described by R_M in the equivalent circuit model. Then, the final equivalent circuit parameters for the two-port resonator can be obtained as

$$C_{0,in} = m\varepsilon_{33}\varepsilon_0 \frac{WL}{T}, \qquad C_{0,out} = m\varepsilon_{33}\varepsilon_0 \frac{WL}{T},$$

$$R_M = \frac{2}{m}\frac{\pi}{8}\frac{T}{L}\frac{\rho_{eq}^{1/2}}{E_{eq}^{3/2}d_{31}^2 Q}, \qquad L_M = \frac{2}{m}\frac{1}{8}\frac{WT}{L}\frac{\rho_{eq}}{E_{eq}^2 d_{31}^2},$$

$$C_M = \frac{m}{2}\frac{8}{\pi^2}\frac{LW}{T}E_{eq}d_{31}^2, \quad N = 1, \quad m = 2 \qquad (2)$$

where m is the number of sub-resonators for each port. The feed-through capacitance C_f added in Fig. 6(c) is used to account for the parasitic capacitances between input and output ports through the substrate, the AlN film and air and it is generally obtained experimentally.

2.5. Filter design

In our filter design, several two-port AlN resonators are connected in series and coupled by their intrinsic capacitance ($C_{0,in}$ and $C_{0,out}$, which are equal in this case and will be denoted by C_0 in the following sections) to realize higher-order filtering. This solution offers the possibility to realize filters with good shape factors and off-band rejection without the need for different frequency devices. The overall equivalent circuit for a self-coupled 3rd order filter is obtained by electrically cascading the models of each two-port resonator, as shown in Fig. 7. The parasitic components (R_{p1}, C_{p1}, R_{p2} and C_{p2}) are added to account for substrate loss and capacitance between the signal and ground electrode lines, which will be neglected in the analytical filter modeling and discussed in more details later.

For this 3rd order electrically coupled filter, three basic resonant modes at different frequencies can be found due to the interactions between the series *RLC* branches and the intrinsic coupling capacitors [13], as illustrated in Fig. 8. In the first resonant mode, all the three *RLC* branches resonate in phase cancelling the effect of coupling capacitors. In the second mode, the first and third *RLC* branches resonate out of phase and each in series with a coupling capacitor, so no current passes through the middle branch.

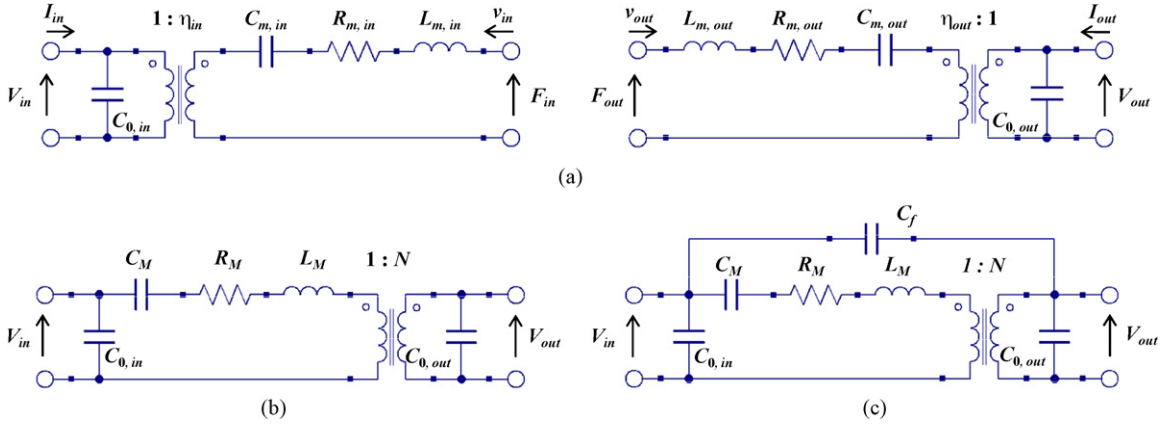

Fig. 6. (a) Equivalent circuit model for input and output sub-resonators. (b) Combined model for a two-port piezoelectric AlN contour-mode resonator. (c) Overall equivalent circuit model of the two-port resonator with feed-through capacitance taken into account.

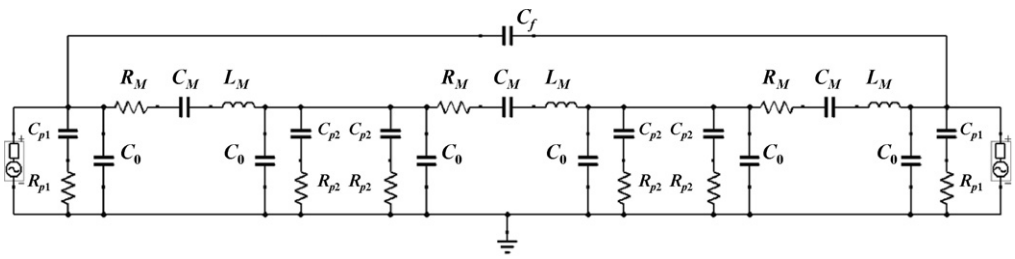

Fig. 7. Overall equivalent circuit model of a 3rd order channel-select filter based on self-coupled piezoelectric AlN contour-mode resonators.

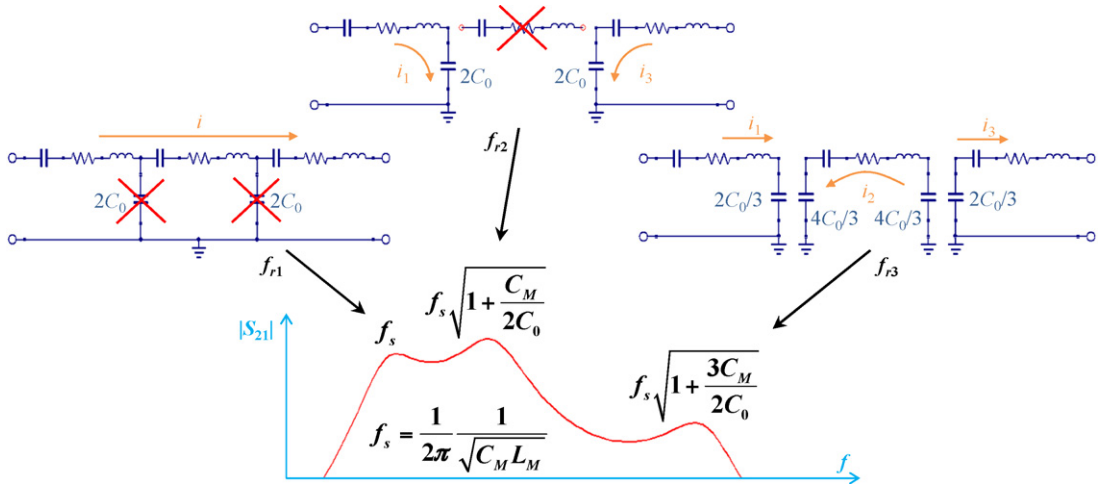

Fig. 8. Three basic resonant modes of a 3rd order electrically coupled filter.

In the third mode, all adjacent branches resonate out of phase with respect to each other and the effect is equivalent to evenly distributing the coupling capacitors among three stages so that the same resonant frequency is obtained for each one. The three corresponding resonant frequencies are given in Fig. 8.

2.5.1. Insertion loss

To maximize power transmission from the input to the output port, the filter needs to be terminated by a proper resistance, R_T, which can be approximated by the impedance magnitude of the input transducer of the first resonator stage. Then, we have

$$R_T \approx \left|\frac{1}{j\omega_s C_0}\right| \tag{3}$$

With good approximation, an nth order filter at resonance is equivalent to a circuit of n series resistors, each having value of R_M, with two additional intrinsic capacitors (C_0) at the two ends, as shown in Fig. 9. By doing some further manipulation and approximation (substituting the expressions of ω_s, C_0, and R_M from Eq. (1) and (2) into Eq. (4)), the filter insertion loss (IL) can be expressed as

$$IL\ [\mathrm{dB}] \approx -20\log_{10}\left(\frac{R_T}{R_T+nR_M}\right) = -20\log_{10}\left(\frac{|1/j\omega_s C_0|}{|1/j\omega_s C_0|+nR_M}\right)$$
$$= -20\log_{10}\left(\frac{4}{4+n\pi^2/k_t^2 Q}\right) \tag{4}$$

where Q is the quality factor of the composing resonators and k_t^2 is the effective electromechanical coupling coefficient [7].

2.5.2. Fractional bandwidth (FBW)

If we use the frequency difference between the first and third resonant modes as an approximation of the 3 dB bandwidth, then the fractional bandwidth (FBW) can be calculated according to the analysis shown in Fig. 8. The result is $\sim 3k_t^2/\pi^2$ which is again a function of the effective electromechanical coupling coefficient and less than half the value that can be obtained by using the ladder topology:

$$FBW_{3\,\mathrm{dB}} \approx \frac{f_{r3}-f_{r1}}{f_{r1}} = \sqrt{\frac{3C_M}{2C_0}+1}-1 \approx \frac{3}{\pi^2}k_t^2 \tag{5}$$

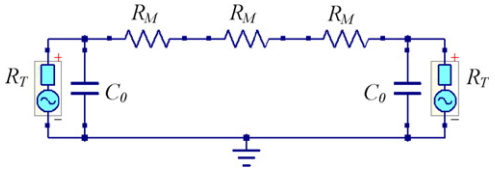

Fig. 9. Equivalent circuit of a 3rd order self-coupled filter at the first resonant mode for the calculation of insertion loss.

2.5.3. Rejection

When out of resonance, the resonators behave as an open circuit and the overall equivalent circuit is given in Fig. 10. Then the out-of-band rejection can be derived as

$$Rej.\ [\mathrm{dB}] \approx -20\log_{10}\left(\frac{C_f}{C_0}\right) - IL \tag{6}$$

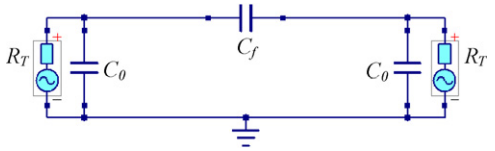

Fig. 10. Equivalent circuit of a 3rd order self-coupled filter out of resonance for the calculation of rejection.

Table 1
Measurement results of channel-select filters based on self-coupled AlN contour-mode resonators.

f_c [MHz]	IL [dB]	$FBW_{3\,dB}$	$Rej.$ [dB]	$SF_{30\,dB}$	$SF_{50\,dB}$	Order	R_T [Ω]
94	5.4	0.2%	60	4.20	8.70	3	800
271	4.2	0.3%	56	3.76	6.61	3	2000
271	5.1	0.3%	60	2.33	5.25	4	2000

f_c: center frequency; IL: insertion loss; $FBW_{3\,dB}$: 3 dB fractional bandwidth; $Rej.$: rejection; SF: shape factor; R_T: termination resistance.

which is primarily determined by the feed-through capacitor C_f and can be controlled by designing the physical distance between the input and output ports.

3. Experimental results

The filters were fabricated using a simple four-mask, low-temperature (<400 °C), potentially post-CMOS compatible process. The two Pt layers were sputter-deposited and patterned by lift-off. The AlN layer in between was sputter-deposited using a Tegal/AMS® PVD tool and exhibits rocking curves as low as 1.2°. The electrical test setup included a Desert Cryogenics® TTP6 probe station, an Agilent® N5230A network analyzer (for 2-port S-parameter measurements), an Agilent® 8562EC Spectrum Analyzer and an Agilent® E8257D PSG Analog Signal Generator (for nonlinearity characterization). The devices under test were directly probed and connected to the measurement instrumentation without the use of any external electronic interface.

3.1. Transmission (S-parameter) measurements

3rd and 4th order channel-select filters at 94 and 271 MHz were tested. The measurement results are summarized in Table 1. The transmission response and photomicrograph of the 3rd order filter at 271 MHz are shown in Fig. 11. Using the circuit model given in Fig. 7, the equivalent device parameters were extracted by fitting the experimental data. C_0 was first estimated from the geometrical parameters of the resonator using Eq. (2), and then the parasitic components (R_{p1}, C_{p1}, R_{p2} and C_{p2}) were extracted from the S-parameter data by subtracting C_0. The extracted values for parasitics were also confirmed by direct measurement of the de-embedding pads fabricated on the same substrate. Given the smaller amount of silicon present in the coupling regions, we assume that R_{p2} and C_{p2} are related to R_{p1} and C_{p1} by a scaling factor s, so that

$$R_{p2} = \frac{R_{p1}}{s}, \qquad C_{p2} = C_{p1} \cdot s \tag{7}$$

This assumption proved to be correct when the final extracted parameters were fitted to the experimental results as shown in Fig. 11(a). At the same time, the extracted resonator parameters also match well with the theoretical values calculated from Eq. (2) based on bulk material properties, shown in Table 2.

Table 2
Comparison of experimentally extracted and theoretically calculated equivalent circuit parameters of the 271 MHz 3rd order filter (the unloaded Q used to compute the theoretical R_M was extracted from the experimental data to be 2100).

	C_M [fF]	L_M [μH]	R_M [Ω]
Theoretical	1.49	230	187
Experimental	1.47	235	188

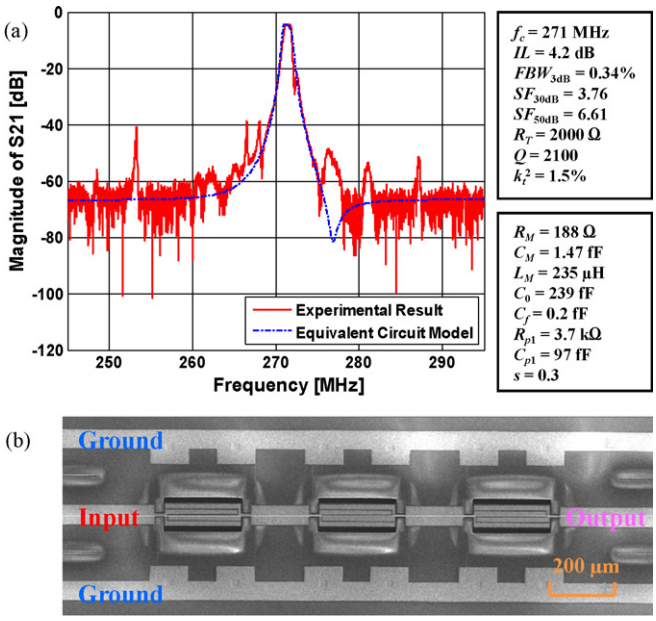

Fig. 11. (a) Transmission response and (b) SEM picture of the 271 MHz 3rd order filter. *Note*: The Q value listed here refers to the quality factor of the composing resonators.

3.2. Influence of substrate parasitics

Since most MEMS devices are fabricated on a Si substrate, parasitic components in the substrate are usually an important factor that influences the device performance. In our case, the MEMS structures were released by a XeF_2 dry etch step, therefore, in this case, a large amount of the silicon was removed except for the regions around the Ground–Signal–Ground (GSG) lines, as illustrated in Fig. 12. Although a high resistivity silicon substrate was used, parasitic components are still present and are modeled by R_p and C_p as shown in Fig. 12. R_p and C_p are just lumped equivalent parameters explaining the physical origin of R_{p1}, C_{p1}, R_{p2} and C_{p2} that have been included in the analytical model of the channel-select filter shown in Fig. 7. For the single-stage two-port resonator design, there are no ground electrodes on the top of the AlN layer that forms the resonator area, as shown in Fig. 3. This is an advantage of this new 2-tether design over the 4-tether design in terms of providing a smoother surface for better AlN deposition. For the testing pads, the ground line is routed from top Pt to bottom Pt by etching the AlN layer and creating via holes (Fig. 12), a process similar to the via connection of metal layers in a CMOS process. Finally the ground line is routed through the bottom side of the tethers (anchors) to the bottom Pt layer underneath the entire resonator.

Using the extracted parameters shown in Fig. 11(a) and Eqs. (4)–(6), the IL, FBW_{3dB}, and $Rej.$ are calculated to be 1.7 dB, 0.49%, and 59 dB, respectively. As we can see, the IL and BW values deviate significantly from the experimental data. This means that the parasitic components play an important role in the filter's performance. On the other hand, since Eqs. (4)–(6) were derived based on a series of approximations, a more accurate numerical simulation was performed to study the effect of parasitics. We found that the IL would reduce to 2.0 dB and the $FBW_{3\,dB}$ would increase to 0.42%, if all the parasitics were to be removed. Therefore, filter performance can be improved to a large extent by reducing the effect of substrate parasitics. It should also be noted that an increase in the $k_t^2 Q$ factor in Eq. (4) would also be able to reduce the IL. This was confirmed by the experimental results shown in Fig. 13, where an improved fabrication process had yielded higher k_t^2 (1.9% instead of 1.5%) and a 3rd order filter with IL of 2.3 dB at 251 MHz. The reduced

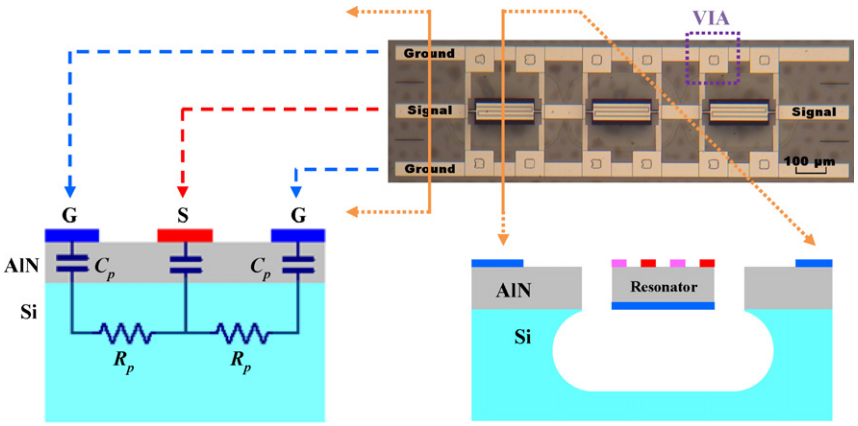

Fig. 12. Illustration of parasitic components in the device substrate.

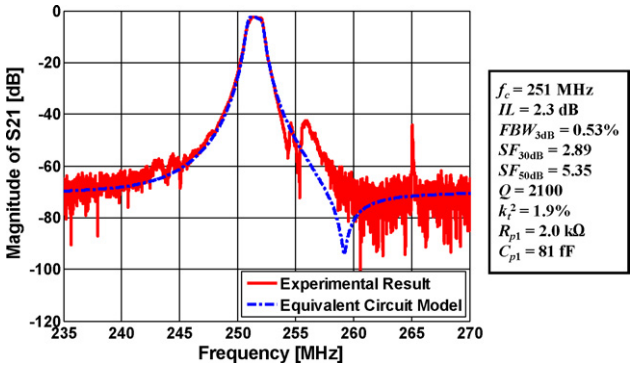

Fig. 13. Response of a 251 MHz 3rd filter showing reduced *IL* of 2.3 dB. *Note*: The *Q* value listed here refers to the quality factor of the composing resonators.

IL is due to the combined effect of primarily higher k_t^2 and partially reduced parasitics of this specific fabrication run. Although not typical, this data point shows that lower losses can be attained with these narrow-band filters and channel-select filtering applications can be targeted.

3.3. Nonlinearity measurements

Two nonlinearity characteristics of the 271 MHz 3rd order filter have been measured: the 1 dB compression point, which was recorded to be 65 dBmV, and the third-order intercept point (IP3). For the measurement of IP3, a two-tone test technique was used [16]. The device under test (DUT, namely the channel-select filter in this case) is fed with two sine tones (two interferers) with frequency differences of $2\cdot\Delta f$ and Δf, respectively, to the filter center frequency, f_c:

$$f_1 = f_c - 2\cdot\Delta f, \qquad f_2 = f_c - \Delta f \tag{8}$$

In this way a third-order intermodulation (IM3) component is generated exactly at the filter center frequency and measured by a spectrum analyzer, as illustrated in Fig. 14. The IP3 intercept point is then obtained graphically by plotting the output power versus the input power both on logarithmic scales (in dB m). Two curves are drawn; one for the linearly filtered signal at the center frequency, and one for the IM3 response. Both curves are extended with straight lines to find the intercept point and therefore the corresponding input and output intercept power values (IIP3 and OIP3), as illustrated in Fig. 14(c).

Depending on the value of Δf, the two interfering tones may be close to or far away from the filter center frequency, and therefore the IIP3 values will change accordingly. For the 271 MHz 3rd order filter, the 3 dB bandwidth was 920 kHz. The measured IIP3 values were recorded to be 92 dBmV, 95 dBmV and 103 dBmV, when Δf is equal to 200 kHz, 400 kHz and 800 kHz, respectively (Fig. 15). These values are different from the data previously reported in [8], but are considered to be more accurate, since, in this setup, attention has been placed to remove any harmonic in the two signal sources (by using low pass filters (LPF) as shown in Fig. 14(a)) and consequently eliminate any second-order intermodulation product. The obtained data confirm that this new filter design shows excellent performance in terms of immunity to intermodulation distortions. The IIP3 values are comparable to existing SAW devices [17] and superior to any similar electrostatically transduced micromechanical device [18]. It is worth noting that the nonlinearity characteristic values are reported as equivalent voltages (dBmV instead of power

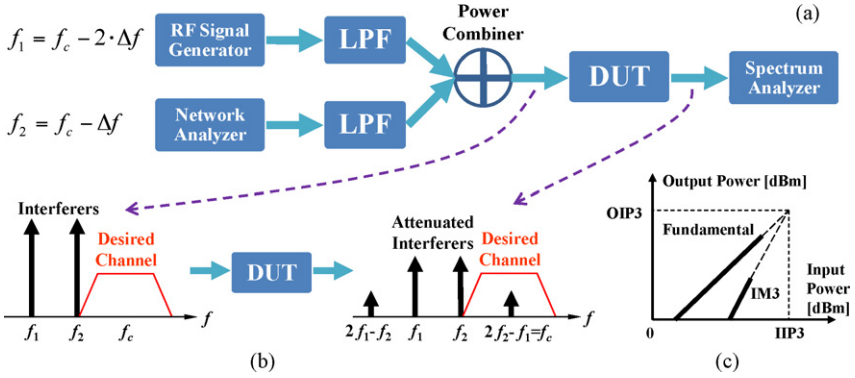

Fig. 14. Illustration of the two-tone technique used to measure the filter IP3.

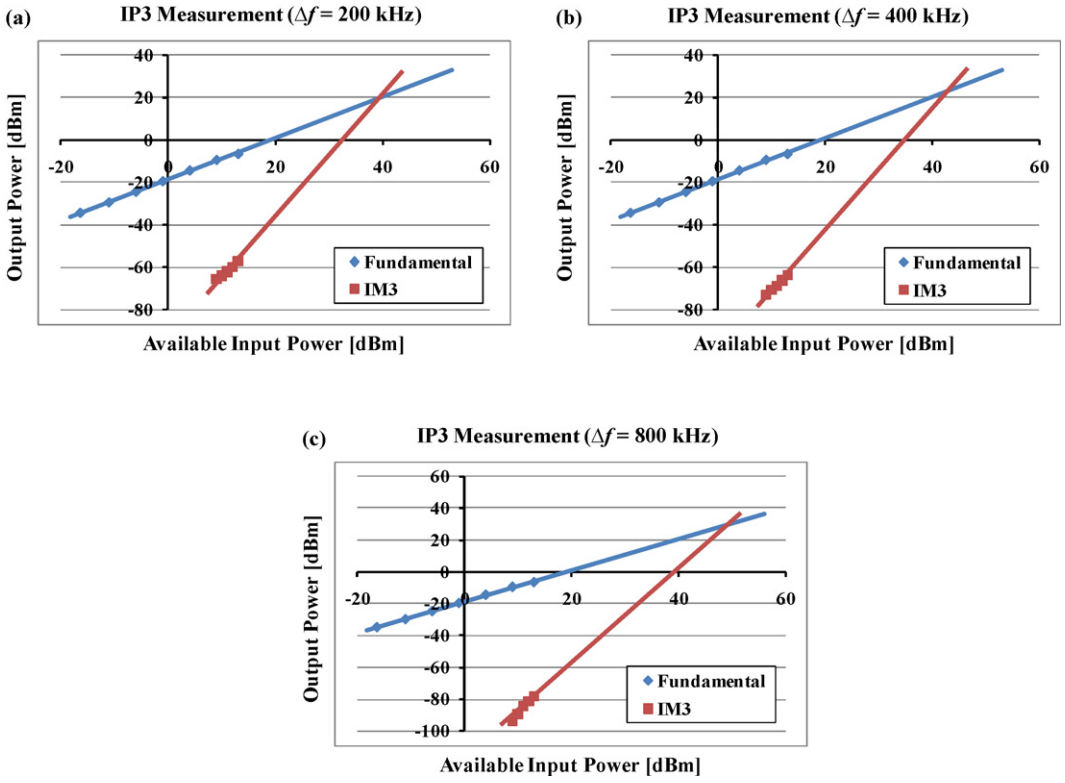

Fig. 15. Measured IP3 data for the 271 MHz 3rd order channel-select filter.

and therefore dB m) that are applied to the piezoelectric transducer. The reason for this choice is because the impedance levels of MEMS devices vary significantly from one technology to another and it would be inadequate to directly compare actual power values.

4. Conclusion

Two-port piezoelectric AlN contour-mode resonators have been connected in series and coupled using their intrinsic capacitance to form multi-frequency, narrow bandwidth, low insertion loss, high off-band rejection and high linearity channel-select filters. To meet the stringent specifications of direct channel selection at the RF stage in future single-chip multi-frequency reconfigurable wireless communications, the self-coupling technique has been proposed and analyzed for the synthesis of narrow-band filters based on the piezoelectric AlN contour-mode MEMS resonators. A thorough discussion on substrate parasitics and their impact on the performance of miniaturized filters at the microscale have been provided together with an improved way of characterizing the third-order nonlinearity of the channel-select filters. Based on this technology and considering that piezoelectric AlN RF MEMS switches [19] have been demonstrated and integrated on the same chip to turn on/off AlN contour-mode resonators and filters, single-chip multi-frequency reconfigurable transceivers and low-power non-traditional RF architectures can be envisioned. Ongoing research is aimed at lowering the termination impedance of the filters, as well as expanding this coupling technique to GHz frequencies.

Acknowledgements

The authors offer special thanks to Philip J. Stephanou and Justin P. Black at Harmonic Devices, and the staff at the Penn Wolf Nanofabrication Lab for their help with part of the fabrication steps.

References

[1] C.T.-C. Nguyen, MEMS technology for timing and frequency control, IEEE Transactions on Ultrasonics, Ferroelectrics and Frequency Control 54 (2) (2007) 251–270.
[2] Y.-W. Lin, S.-S. Li, Z. Ren, C.T.-C. Nguyen, Vibrating micromechanical resonators with solid dielectric capacitive transducer gaps, in: Joint IEEE International Frequency Control/Precision Time & Time Interval Symposium, Vancouver, Canada, August, 2005, pp. 128–134.
[3] D. Weinstein, S.A. Bhave, Internal dielectric transduction of a 4.5 GHz silicon bar resonator, in: IEEE International Electron Devices Meeting (IEDM 2007), Washington, DC, December, 2007, pp. 415–418.
[4] G. Piazza, P.J. Stephanou, A.P. Pisano, Piezoelectric aluminum nitride vibrating contour-mode MEMS resonators, Journal of MicroElectroMechanical Systems 15 (December (6)) (2006) 1406–1418.
[5] G.K. Ho, R. Abdolvand, A. Sivapurapu, S. Humad, F. Ayazi, Piezoelectric-on-silicon lateral bulk acoustic wave micromechanical resonators, Journal of MicroElectroMechanical Systems 17 (April (2)) (2008) 512–520.
[6] R. Ruby, P. Bradley, J. Larson III, Y. Oshmyansky, D. Figueredo, Ultra-miniature high-Q filters and duplexers using FBAR technology, in: 2001 IEEE International Solid-State Circuits Conference, February, 2001, pp. 121–122.
[7] G. Piazza, P.J. Stephanou, A.P. Pisano, Single-chip multiple-frequency AlN MEMS filters based on contour-mode piezoelectric resonators, Journal of MicroElectroMechanical Systems 16 (April (2)) (2007) 319–328.
[8] C. Zuo, N. Sinha, M.B. Pisani, C.R. Perez, R. Mahameed, G. Piazza, Channel-select RF MEMS filters based on self-coupled AlN contour-mode piezoelectric resonators, in: 2007 IEEE International Ultrasonics Symposium, New York, USA, October, 2007.
[9] H.-Y. Tsui, J. Lau, A 5 GHz 56 dB voltage gain 0.18 μm CMOS LNA with built-in tunable channel filter for direct conversion 802.11a wireless LAN receiver, in: 2003 IEEE Radio Frequency Integrated Circuits (RFIC) Symposium, Philadelphia, PA, USA, June, 2003, pp. 225–228.
[10] S. Kiaei, S.M. Taleie, B. Bakkaloglu, Low-power high-Q NEMS receiver architecture, in: 2005 IEEE International Symposium on Circuits and Systems (ISCAS 2005), vol. 5, May, 2005, pp. 4401–4404.
[11] R. Ruby, P. Bradley, J.D. Larson III, Y. Oshmyansky, PCS 1900 MHz duplexer using thin film bulk acoustic resonator (FBARs), Electronics Letters 35 (10) (1999) 794–795.
[12] H. Chandrahalim, D. Weinstein, L.F. Cheow, S.A. Bhave, High-κ dielectrically transduced MEMS thickness shear mode resonators and tunable channel-select RF filters, Sensors and Actuators A 136 (2007) 527–539.
[13] S. Pourkamali, F. Ayazi, Electrically coupled MEMS bandpass filters. Part I. With coupling element, Sensors and Actuators A 122 (2005) 307–316.
[14] G. Piazza, P.J. Stephanou, A.P. Pisano, One and two port piezoelectric higher order contour-mode MEMS resonators for mechanical signal processing, Solid-State Electronics 51 (2007) 1596–1608.

[15] G. Piazza, A.P. Pisano, Dry-released post-CMOS compatible contour-mode aluminum nitride micromechanical resonators for VHF applications, in: 2004 Solid State Sensor, Actuator and Microsystems Workshop (Hilton Head 2004), Hilton Head Island, SC, USA, 2004, pp. 37–40.
[16] R. Navid, J.R. Clark, M. Demirci, C.T.-C. Nguyen, Third-order intermodulation distortion in capacitively-driven CC-beam micromechanical resonators, in: The 14th IEEE International Conference on Micro Electro Mechanical Systems (MEMS 2001), January, 2001, pp. 228–231.
[17] Y. Satoh, O. Ikata, T. Miyashita, H. Ohmori, RF SAW filters, in: International Symposium on Acoustic Wave Devices for Future Mobile Communication Systems, March, 2001, pp. 125–132.
[18] A.T. Alastalo, V. Kaajakari, Third-order intermodulation in microelectromechanical filters coupled with capacitive transducers, Journal of MicroElectroMechanical Systems 15 (February (1)) (2006) 141–148.
[19] R. Mahameed, N. Sinha, M.B. Pisani, G. Piazza, Dual-beam actuation of piezoelectric AlN RF MEMS switches monolithically integrated with AlN contour-mode resonators, Journal of Micromechanics and Microengineering 18 (2008), 105011 (11 pp.).

Biographies

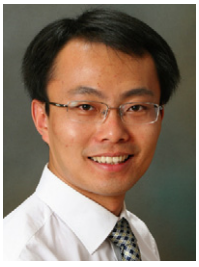

Chengjie Zuo received his B.S. in Electronic Information Science and Technology from the University of Science and Technology of China (USTC), Hefei, Anhui, China in 2004 and a M.Sc. in Electrical Engineering with Honors from the Delft University of Technology (TU Delft), Delft, Netherlands in 2006. He is currently working toward his Ph.D. degree in Electrical and Systems Engineering at the University of Pennsylvania in Philadelphia, PA. His primary research interests are Micro/Nano ElectroMechanical Systems (MEMS/NEMS) devices, analog and RF integrated circuits (IC), and MEMS-IC integration and co-design. He was the recipient of the Best Student Paper Award in the Oscillators, Synthesizers, and Noise group at the 2008 IEEE International Frequency Control Symposium and the IEEE Solid-State Circuits Society Predoctoral Fellowship for 2009–2010. He was also a co-recipient of the Best Student Paper Award in the Materials, Filters, and Resonators group and a finalist in the Oscillators, Synthesizers, Noise, and Circuit Techniques group at the 2009 Joint Meeting of the European Frequency and Time Forum and the IEEE International Frequency Control Symposium.

Nipun Sinha is currently working towards his Ph.D. degree in the Department of Mechanical Engineering and Applied Mechanics at the University of Pennsylvania, Philadelphia. He received his B.Eng. from Punjab Engineering College, Chandigarh, India in 2004 and his M.S. from Texas A&M University, College Station in 2006, both in Mechanical Engineering. He has worked at Indian Institute of Technology (IIT), Delhi and at the Indian Oil Corporation Research and Development Centre, Faridabad, India as a Research Trainee. In his masters' studies, at the Texas A&M University, he performed research in the Multi-Phase Flow and Heat Transfer Laboratory where he worked on the development of thin-film thermocouples for studying boiling. His present research in the Penn Micro and Nano Systems (PMaNS) Lab focuses on piezoelectric micro and nano switches (MEMS/NEMS) for RF wireless communications and nano computing applications, development of piezo-nanoactuators and integration of micro/nanoswitches with wireless components. He also has general interest in the areas of micro/nanofabrication techniques, surface characterization techniques, thin-film characterization, heat transfer, fluid mechanics and bio-nanotechnology.

Gianluca Piazza is a Wilf Family Term Assistant Professor in the department of Electrical and Systems Engineering (ESE) at the University of Pennsylvania. His research interests focus on piezoelectric micro and nano systems (MEMS/NEMS) for RF wireless communications, biological detection, wireless sensor platforms and all mechanical computing. He also has general interest in the areas of micro/nano fabrication techniques and integration of micro/nano devices with state-of-the-art electronics. He received his Ph.D. degree from the University of California, Berkeley where he developed a new class of AlN contour-mode vibrating microstructures for RF communications. He has more than 10 years of experience working with piezoelectric materials. He holds two patents in the field of micromechanical resonators and has recently co-founded a start-up (Harmonic Devices, Inc.) aiming at the commercialization of single-chip and multi-band RF filters and oscillators. He received the IBM Young Faculty Award in 2006 and has won, with his students, the Best Paper Award in Group 1 and 2 at the IEEE Frequency Control Symposium in 2008 and 2009, respectively.